Matrix effects on copper(II)phthalocyanine complexes. A combined continuous wave and pulse EPR and DFT study†

Cinzia Finazzo,‡[a] Carlos Calle,‡[a] Stefan Stoll,[a] Sabine Van Doorslaer*[b] and Arthur Schweiger§[a]

Received 14th November 2005, Accepted 28th February 2006
First published as an Advance Article on the web 15th March 2006
DOI: 10.1039/b516184c

The effect of the electron withdrawing or donating character of groups located at the periphery of the phthalocyanine ligand, as well as the influence of polar and nonpolar solvents are of importance for the redox chemistry of metal phthalocyanines. Continuous wave and pulse electron paramagnetic resonance and pulse electron nuclear double resonance spectroscopy at X- and Q-band are applied to investigate the electronic structure of the complexes Cu^{II}phthalocyanine (CuPc), copper(II) 2,9,16,23-tetra-*tert*-butyl-29*H*,31*H*-phthalocyanine ($CuPc^t$), and copper(II) 1,2,3,4,8,9,10,11,15,16,17,18,22,23,24,25-hexadecafluoro-29*H*,31*H*-phthalocyanine ($CuPc^F$) in various matrices. Isotope substitutions are used to determine the *g* values, the copper hyperfine couplings and the hyperfine interactions with the ^{14}N, ^{1}H and ^{19}F nuclei of the macrocycle and the surrounding matrix molecules. Simulations and interpretations of the spectra are shown and discussed, and a qualitative analysis of the data using previous theoretical models is given. Density functional computations facilitate the interpretation of the EPR parameters. The experimental *g*, copper and nitrogen hyperfine and nuclear quadrupole values are found to be sensitive to changes of the solvent and the structure of the macrocycle. To elucidate the electronic, structural and bonding properties the changes in the *g* principal values are related to data from UV/Vis spectroscopy and to density functional theory (DFT) computations. The analysis of the EPR data indicates that the in-plane metal–ligand σ bonding is more covalent for $CuPc^t$ in toluene than in sulfuric acid. Furthermore, the out-of-plane π bonding is found to be less covalent in the case of a polar sulfuric acid environment than with nonpolar toluene or H_2Pc environment, whereby the covalency of this bonding is increased upon addition of *tert*-butyl groups. No contribution from in-plane π bonding is found.

Introduction

The phthalocyanine (Pc) macrocycle (Fig. 1) is a synthetic analogue of the porphyrin macrocycle. Around seventy different metal ions can be placed in the central cavity of Pc and the choice of this cation can strongly influence the physical properties of the metal phthalocyanines. Many of the metal ions (*e.g.* Cu^{II}, Co^{II}, Fe^{II}) are held so tightly that they cannot be removed without the destruction of the macrocycle.

Phthalocyanines and metal phthalocyanines (MPc) are used in industry in a variety of applications ranging from conventional dyes to catalysis, or from coatings for read/write CD-RWs to anti-cancer agents. Their extremely high thermal stability, inertness to acids and alkalis, insolubility in most solvents, high dyeing power, and color intensity have ensured their reputation and wide application in the painting, printing, textile, and paper industries, as well as in chemical fibre and plastic dyeing processes.[1–3] Due to their photocatalytic activities[4] these compounds are also applied as oxidation–reduction catalysts[5] in industrial synthesis, enzyme catalysis, and the electrochemical reduction of oxygen and water in fuel cells.[6–8] Several electrically conducting phthalocyanines are used in commercial electronic devices.[9] Furthermore, phthalocyanines are applied in the production of heavy isotopes and are used as corrosion inhibitors.[6]

Metal-free phthalocyanine and the majority of its divalent metallic derivatives have limited solubility in most solvents except in sulfuric acid. The solubility in common organic solvents can be greatly increased by placing substituents on the Pc ring at peripheral (p = 2, 3, 9, 10, 16, 17, 23, 24) and non-peripheral (np = 1, 4, 8, 11, 15, 18, 22, 25) benzo sites. The ring substituents reduce the intermolecular attractions between the Pcs in the crystalline form, thereby increasing their solubility. Note that in this paper we use the phthalocyanine nomenclature given in ref. 6.

[a] *Physical Chemistry Laboratory, ETH Zurich, 8093 Zurich, Switzerland*
[b] *SIBAC Laboratory - Department of Physics, University of Antwerp, Universiteitsplein 1, 2610 Wilrijk, Belgium. E-mail: sabine.vandoorslaer@ua.ac.be; Fax: (+32)38202470*

† Electronic supplementary information (ESI) available: UV/Vis data for CuPc, $CuPc^t$, and $CuPc^F$ in H_2SO_4 and $CuPc^t$ in toluene (Table S1); experimental and simulated X-band cw-EPR spectra of $CuPc^t$ in H_2SO_4 and CuPc in H_2Pc (Fig. S1); experimental and simulated Q-band cw-EPR spectra of CuPc in H_2SO_4 and H_2Pc and $CuPc^t$ in toluene (Fig. S2); experimental and simulated X- and Q-band Davies-ENDOR spectra of CuPc in H_2SO_4 and H_2Pc, and $CuPc^t$ in toluene (Fig. S3); spin density on the CuPc complex obtained from DFT calculations (Fig. S4). See DOI: 10.1039/b516184c

‡ These authors contributed equally to this work.

§ Deceased on 4 January 2006.

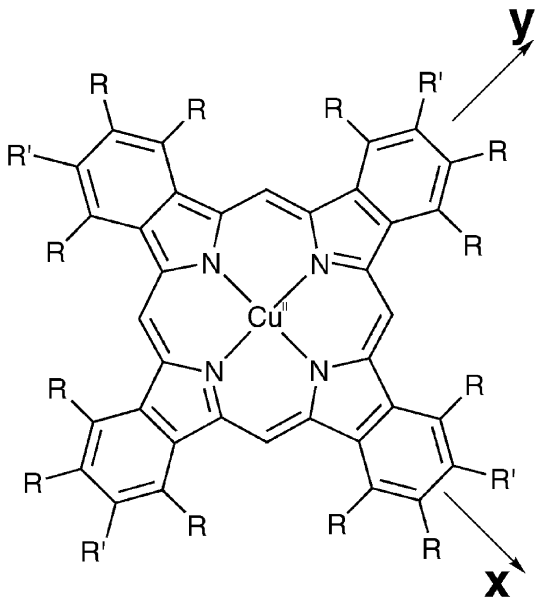

Fig. 1 Structure of Cu^{II}phthalocyanine (CuPc, R = R′ = H) and the related complexes $CuPc^t$ (R′ = *tert*-butyl, R = H) and $CuPc^F$ (R = R′ = F), with the definition of the axes used in the analysis.

In view of the different industrial applications of MPcs, the influence of the benzo-substituents and the solvent on the characteristics of the complexes should be known. It has been demonstrated that the introduction of appropriate electron-donating and -withdrawing substituents in the Pc macrocycle allows for a fine-tuning of the electronic structure. In the case of paramagnetic MPcs, the ***g*** matrix and the spin density distribution, which influences its catalytic activity, can be determined using electron paramagnetic resonance (EPR) spectroscopy.

Most EPR investigations on MPcs done so far used continuous wave (cw) EPR.[10–18] The results are partially contradictory and many of the magnetic parameters are still not known. During the last two decades, different pulse EPR and electron nuclear double resonance (ENDOR) techniques[19–21] have been developed, which allow for a much more detailed investigation of the influences of matrix molecules and ring substituents on the spin-density distribution in these complexes.

In this work, we present a cw and pulse EPR and ENDOR study of the Cu^{II} complexes of Pc, 2,9,16,23-tetra-*tert*-butyl-29*H*, 31*H*-phthalocyanine (Pc^t), and 1,2,3,4,8,9,10,11,15,16,17,18,22,23,24,25-hexadecafluoro-29*H*, 31*H*-phthalocyanine (Pc^F) in various matrices. By means of cw-EPR, hyperfine sublevel correlation[22] (HYSCORE) and Davies- and Mims-ENDOR[23,24] spectroscopy at X- and Q-band[25] frequencies in combination with isotope substitutions, the *g* values, copper hyperfine couplings and hyperfine interactions of the ^{14}N, ^{1}H and ^{19}F nuclei of the macrocycle and the surrounding matrix molecules are determined and discussed. The hyperfine and nuclear quadrupole couplings of the isoindole nitrogens and the copper hyperfine values are found to be sensitive to the solvent and the type of ring substituents. Moreover, clear changes were observed in the proton-ENDOR spectra upon changes or deuteration of the solvent. The use of deuterated solvents shows that sulfuric acid, which is often used as a solvent for metal phthalocyanines, interacts with the CuPc complexes. Moreover, in the preparation of CuPc magnetically diluted in H_2Pc, great care has to be taken to remove all sulfuric acid by vacuum sublimation. This becomes obvious from spectral comparison with the data of CuPc in sulfuric acid. In view of this finding, some of the results presented in the literature have to be revised. Furthermore, the motional behaviour of $CuPc^t$ in toluene is found to be different to that in sulfuric acid.

For the design of new MPc materials, it is of importance to evaluate the effect of electron-donating and electron-withdrawing peripheral and non-peripheral substituents in the macrocycle and to assess the influence of the different solvents on the electronic structure of the complexes. Our present investigation shows that advanced EPR techniques provide very sensitive tools to probe these effect.

Experimental

Sample preparation

CuPc, $CuPc^t$, $CuPc^F$, and phthalocyanine (H_2Pc) (98%) were obtained from Aldrich. Sulfuric acid (Merck, 98% suprapure) and toluene (Fluka, puriss., absolute, over molecular sieves) were used as solvents. Deuterated sulfuric acid (D_2SO_4) and toluene-d_8 (>99.6% purity) were obtained from Cambridge Isotope Laboratories (CIL). Since the commercially available compounds are not of sufficient purity for EPR studies, CuPc, $CuPc^t$, $CuPc^F$, and H_2Pc were washed successively with water, acetone and ethanol in a Soxhlet apparatus to remove organic impurities, and dried at 80 °C overnight. The dried products were then further purified by vacuum evaporation for 1 h (10^{-5} mbar). CuPc and $CuPc^F$ were dissolved in sulfuric acid and in D_2SO_4 to a concentration of 10^{-3} M. $CuPc^t$ was dissolved in sulfuric acid, D_2SO_4, toluene or toluene-d_8 to a concentration of 10^{-3} M. The magnetically diluted compound CuPc : H_2Pc (1 : 500 weight ratio) was prepared according to Abkowitz *et al.*[11] The sulfuric acid was removed by sublimation and the β-form was isolated.[26,27]

Optical spectroscopy

The UV/Vis spectra were recorded at room temperature with a Perkin Elmer Lambda 900 spectrophotometer between 200 and 900 nm with a scan rate of 375 nm min^{-1}. In addition to CuPc, reference spectra of sulfuric acid and toluene solutions were measured to allow for a baseline correction of the copper phthalocyanine complexes.

EPR spectroscopy

The X-band cw-EPR spectra were recorded at 110 K on a Bruker ESP300 spectrometer (microwave (mw) frequency, 9.43 GHz) equipped with a liquid nitrogen cooling system. A mw power of 20 mW, modulation amplitude of 0.5 mT and

modulation frequency of 100 kHz were used. Solution spectra at room temperature were measured using a flat cell (mw frequency 9.81 GHz). The X-band pulse ENDOR and EPR experiments (repetition rate 1 kHz) were carried out with a Bruker Elexsys spectrometer (mw frequency 9.73 GHz) equipped with a helium cryostat from Oxford Inc. (temperature 15 K). The spectra were recorded at different observer positions to analyze all the molecular orientations (orientation selectivity[28]).

The HYSCORE spectra[22] were measured with the pulse sequence $\pi/2$-τ-$\pi/2$-t_1-π-t_2-$\pi/2$-τ-echo, with pulse lengths $t_{\pi/2}$ = 24 ns and t_π = 16 ns. Two τ values, 96 and 344 ns, were used and the time intervals t_1 and t_2 were varied from 96–8272 ns in steps of 16 ns. An eight-step phase cycle was used to eliminate unwanted echoes.[29]

Mims-ENDOR spectra[24] were recorded using the mw pulse sequence $\pi/2$-τ-$\pi/2$-T-$\pi/2$-τ-echo, with pulse lengths of 16 ns. A selective radio frequency (rf) pulse with variable frequency ν_{rf} and a length of 10 μs was applied during the time interval T. The rf increment was 50 kHz, and time τ was varied from 120–280 ns in steps of 8 ns to avoid signal distortions due to blind spots.

Davies-ENDOR spectra[23] were measured with the mw sequence π-T-$\pi/2$-τ-π-τ-echo with a time interval of τ = 900 ns. To detect weakly coupled ^{1}H (strongly coupled ^{14}N) nuclei mw pulses with a length of $t_{\pi/2}$ = 200 (26) ns and t_π = 400 (52) ns were used. An rf π pulse of variable frequency ν_{rf} and lengths 10 (5.4) μs was applied during time T. The rf increment was set to 25 (50) kHz.

Q-Band cw-EPR and pulse-ENDOR spectra were recorded using a laboratory-built pulse-EPR spectrometer (mw frequency 35.30 GHz).[25] Davies-ENDOR experiments were carried out at 25 K with a repetition rate of 200 Hz. Mw pulses with a length of $t_{\pi/2}$ = 20 ns and t_π = 40 ns and a time interval τ = 220 ns were used. An rf π pulse of variable frequency ν_{rf} and lengths 25 μs was applied during time T. The rf increment was set to 50 kHz.

Data manipulation and simulations

The data were processed with the program MATLAB 6.1 (The MathWorks, Inc., Natick, MA). The time traces of the HYSCORE spectra were baseline corrected with a third-order polynomial, apodized with a Hamming window and zero filled. After a two-dimensional (2D) Fourier transformation, the absolute value spectra were calculated. In order to eliminate the τ-dependent blind spots appearing in the HYSCORE and Mims-ENDOR spectra, the spectra taken at different τ values have been added. The cw-EPR, Davies- and Mims-ENDOR spectra were simulated using the program EasySpin written in-house (http://www.esr.ethz.ch).[30]

DFT computations

Spin-unrestricted density functional theory (DFT) computations of hyperfine and nuclear quadrupole couplings were performed with the Amsterdam Density Functional (ADF 2003.01) package.[31–34] The geometry optimizations were done using the RPBE functional together with a Slater-type basis set of triple-ζ quality and a single set of polarization functions (TZP, old name: basis set IV). For the calculations of the hyperfine and nuclear quadrupole parameters in ADF, we also used the RPBE functional and a triple-ζ basis set with double polarization functions with the zeroth-order regular approximation (TZ2P, formerly known as basis set ZORA V).[35] For each computation step solvent effects have been taken into account by applying the conductor like screening model (COSMO) of solvation.[36] A fourfold protonation of the meso nitrogen nuclei has been applied for the calculations of the phthalocyanine complexes in sulfuric acid in agreement with previous experimental findings.[37–40]

The dielectric constants were taken from ref. 41. A spin density cube was generated with 0.5 b (coarse grid) resolution using the auxiliary program DENSF within the ADF package. The visualization of the spin density was performed with Molekel.[42] The hyperfine tensors have been visualized using a MATLAB-based program written in-house.

Theoretical background of EPR spectroscopy

The spin Hamiltonian of a system with a Cu^{II} ion (electronic configuration $3d^9$, S = 1/2, I = 3/2), ^{14}N (I = 1), ^{19}F and ^{1}H (I = 1/2) nuclei (in frequency units) is given by

$$H_0 = \frac{\beta_e \tilde{\boldsymbol{B}}_0 \boldsymbol{g} \boldsymbol{S}}{h} + \tilde{\boldsymbol{S}} \boldsymbol{A}^{\mathrm{Cu}} I + \sum_i \tilde{\boldsymbol{S}} \boldsymbol{A}_i^N I_i + H_{\mathrm{nucl}}. \qquad (1)$$

The first term is the electron Zeeman interaction with the external magnetic field vector $\boldsymbol{B}_0$ and the second term represents the hyperfine interaction between the electron spin S and the nuclear spin I of the copper nucleus (^{63}Cu, ^{65}Cu). The third term describes the hyperfine interactions with the isoindole nitrogen nuclei, whereas the last term describes all the remaining hyperfine and nuclear quadrupole interactions of the surrounding nuclei. For CuPc complexes, the $\boldsymbol{g}$ and $\boldsymbol{A}^{\mathrm{Cu}}$ matrices are assumed to be axially symmetric and coaxial. The cw-EPR spectra are dominated by the first three terms in eqn (1). The hyperfine and nuclear quadrupole parameters of the isoindole nitrogens and the proton and ^{19}F hyperfine couplings can be determined using ENDOR, whereas the interactions with the four remote nitrogens can be inferred from electron spin echo envelope modulation (ESEEM) experiments. In general, a hyperfine matrix $\boldsymbol{A}$ can be written as the sum of an isotropic hyperfine coupling, a_{iso}, and an anisotropic part, which can often be described by the point-dipole approximation. In this case, the elements of the hyperfine matrix are given by

$$A_{ij} = a_{\mathrm{iso}}\delta_{ij} + \frac{\mu_0}{4\pi}\frac{g_n\beta_e\beta_n}{r^3 h} g_i(3r_i r_j - \delta_{ij})(i,j = x,y,z) \qquad (2)$$

which depends on the distance r between the unpaired electron and the nucleus.[43] For an axial $\boldsymbol{g}$ matrix, ($g_x = g_y = g_\perp$, $g_z = g_\parallel$), $l_x = \sin\phi$, $l_y = 0$, and $l_z = \cos\phi$ with ϕ defining the angle between the $g_\parallel$ principal axis and the vector $\boldsymbol{r}$.

The nuclear quadrupole tensor $\boldsymbol{Q}$ is traceless, with principal values $Q_x = [-(e^2qQ/4h)]\,(1-\eta)$, $Q_y = [-(e^2qQ/4h)]\,(1+\eta)$, and $Q_z = e^2qQ/2h = 2K$, where η is the asymmetry parameter.

Results

The UV/Vis spectra of CuPc, $CuPc^t$ and $CuPc^F$ in sulfuric acid and of $CuPc^t$ in toluene (not shown) exhibit strong absorptions in the Q-band and the B-band (or Soret band) (see Table S1 of the ESI†). The dominant Q-band absorption, responsible for the characteristic blue color of the complexes, can be assigned to a π–π* transition from the highest occupied molecular orbital (HOMO) of a_{1u} symmetry, to the lowest unoccupied molecular orbital (LUMO) of e_g symmetry.[44] This band splits when the complex has a symmetry lower than D_{4h}. The Q-bands split also upon protonation of the meso nitrogen nuclei. Non-peripheral substitution greatly influences the Q-band absorption, whereas peripheral substitution (such as in $CuPc^t$) has a smaller effect on the position of the Q-band.[6] The copper d–d absorption band largely overlaps the π–π* absorption bands of the organic ring, which has an extinction coefficient of 10^4 higher than the one of the d–d absorption bands.[16] Therefore, d–d transition energies have to be assessed by other spectroscopic methods such as EPR. From the UV/Vis spectrum of $CuPc^F$ in sulfuric acid it could be seen that even after vacuum sublimation the sample is not pure (see also later).

The X-band cw-EPR spectra of CuPc and $CuPc^t$ recorded in different matrices at 120 K are shown in Fig. 2a and b and Fig. S1 of the ESI.† The spectra are axially symmetric with resolved copper hyperfine splittings (isotopes ^{63}Cu and ^{65}Cu). These features are further split due to the hyperfine interaction with the four geometrically equivalent isoindole nitrogen nuclei ($I = 1$). Based on symmetry considerations, the $g_\parallel$ axis is oriented perpendicular to the phthalocyanine plane (along the molecular z-axis). The other two axes of the molecular frame are taken as indicated in Fig. 1. The spectrum of CuPc in H_2Pc shows a strong signal of a free radical (see Figure S1b†). This signal has also been observed in other CuPc samples.[10,11,13,45]

The g values can be more accurately determined at Q-band (Fig. 2c and Fig. S2 of the ESI†). The spectral features corresponding to the two principal g values ($g_\parallel$ and $g_\perp$) overlap in the X-band spectra. In the Q-band EPR spectra they are fully separated. Since in the $g_\perp$ region the copper and nitrogen hyperfine couplings are of the same order of magnitude (Fig. 2, Fig. S1 and S2†), $A_\perp^{Cu}$ is difficult to determine. For CuPc and $CuPc^t$ in liquid solutions, the isotropic copper hyperfine coupling can in principle be evaluated from the room temperature EPR spectra. From the knowledge of these parameters together with the clearly resolved $A_\parallel^{Cu}$ splittings observed in the cw-EPR spectra of the frozen solutions, the $A_\perp^{Cu}$ values can then be deduced.

Fig. 3a shows that this procedure is indeed successful for $CuPc^t$ in toluene, where the rotational correlation time is less then 0.3 ns. However, the EPR spectra of CuPc and $CuPc^t$ in sulfuric acid recorded at room temperature in a flat cell do not show an averaging of the signal. Possible explanations for this finding are: (i) the surface of the flat cell orients the CuPc molecules with their plane parallel to the surface, (ii) the CuPc molecules undergo a complicated rotational motion (slow motion regime for rotations around the in-plane axes) mainly due to the high viscosity of the solvent, or (iii) the torque on the molecule caused by the magnetic field due to the g anisotropy is sufficiently strong to orient the molecules. Option (i) was excluded by using a capillary instead of a flat cell. Option (iii) could be discarded by freezing the sample

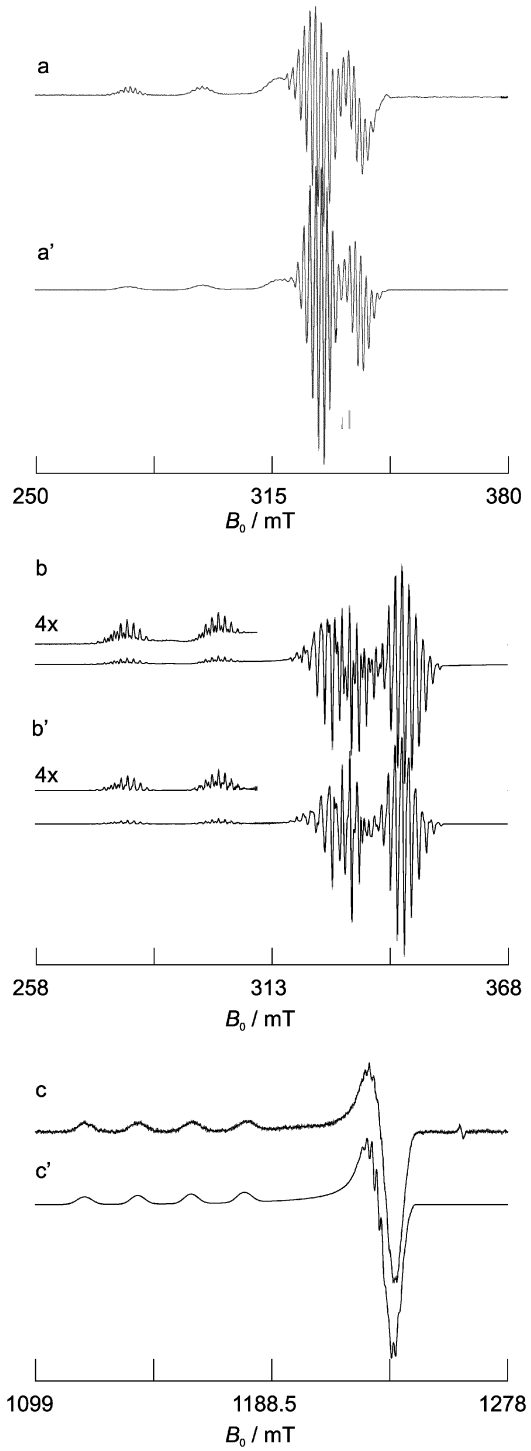

Fig. 2 Experimental and simulated X-band cw-EPR spectra recorded at 120 K, (a) CuPc in sulfuric acid and (b) $CuPc^t$ in toluene. (c) Experimental and simulated Q-band cw-EPR spectrum of $CuPc^t$ in sulfuric acid obtained at 120 K. The simulated spectra are denoted by a′, b′ and c′.

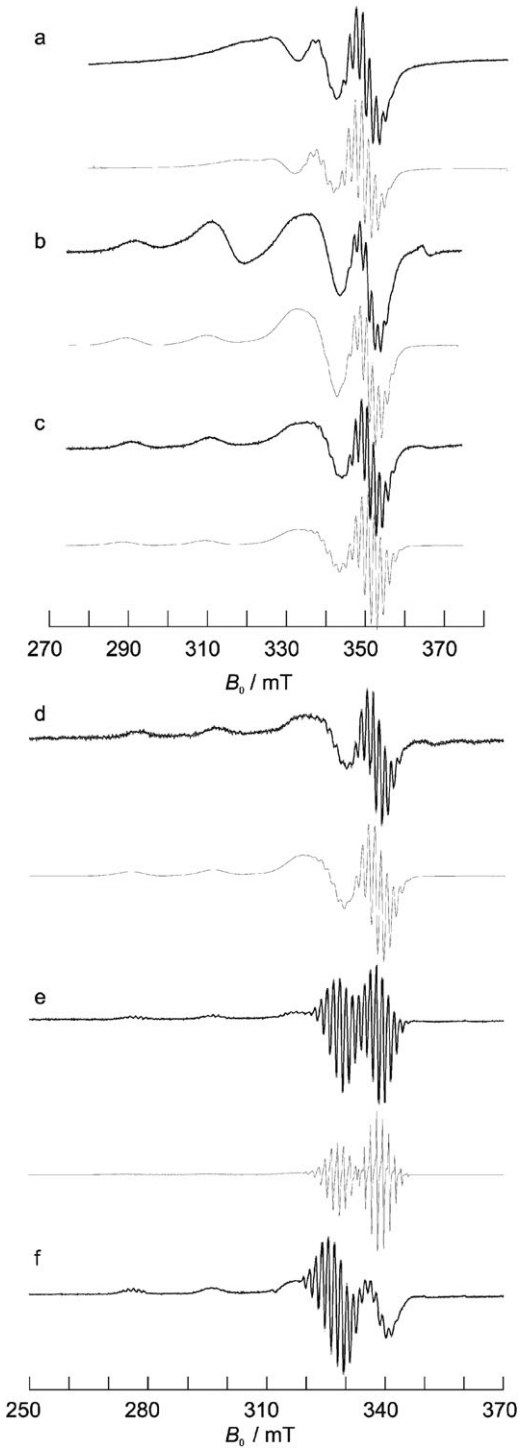

Fig. 3 Experimental X-band cw-EPR spectra recorded at room temperature in a flat cell. (a) $CuPc^t$ in toluene. (b) CuPc in sulfuric acid. (c) $CuPc^t$ in sulfuric acid. Experimental X-band cw-EPR spectra of $CuPc^t$ in sulfuric acid in a capillary at (d) 295, (e) 235 and (f) 200 K. The simulated spectra of (a)–(e) are shown below the experimental data in grey. The fast motion (a) and slow motion spectra (b)–(f) were simulated using EasySpin.[30] The simulation of the rigid limit spectrum (f) is not shown here.

while the field was applied (Fig. 3d–f). Upon lowering the temperature from 295 to 235 K, the rotational correlation time changes from 44 ns to 1 μs, approaching the rigid limit (see the ESI for the exact simulation data†). Below 235 K, the full powder spectrum is observed (Fig. 3f). This behaviour reflects the slowing down of the molecular motion upon freezing and confirms case (ii).

The g and A^{Cu} parameters obtained from simulations of the experimental cw-EPR spectra (Fig. 2) are collected in Table 1. The sign of the copper hyperfine values is taken to be negative in accordance with earlier studies on copper complexes[47] and with the DFT results (see Table 4).

To determine the hyperfine and nuclear quadrupole principal values of the isoindole nitrogens, Davies-ENDOR spectra at X- and Q-band were recorded for different settings of the magnetic field. Fig. 4 shows the X-band nitrogen Davies-ENDOR spectra of CuPc and $CuPc^t$ in different matrices taken at observer position $\boldsymbol{B}_0 \parallel g_\perp$. The spectra were recorded using hard mw pulses in order to suppress the ENDOR signals of weakly coupled protons. Both the matrix and macrocycle substituents affect the hyperfine and nuclear quadrupole couplings of the isoindole nitrogens. The ENDOR signals shift to lower frequencies upon going from a relatively inert matrix (toluene or H_2Pc) to the polar sulfuric acid.

Fig. 5 shows the X-band and Q-band nitrogen Davies-ENDOR spectra of $CuPc^t$ in sulfuric acid recorded at the high-field position ($\boldsymbol{B}_0 \parallel g_\perp$), and the low-field position ($\boldsymbol{B}_0 \parallel g_\parallel$, $m_I = -3/2$) together with the corresponding simulations. Fig. S3 of the ESI shows similar experimental and simulated nitrogen ENDOR spectra for $CuPc^t$ in toluene and CuPc in sulfuric acid and H_2Pc.† From the Q-band ENDOR spectra at $\boldsymbol{B}_0 \parallel g_\perp$, the values A_x, A_y, Q_x, Q_y can be derived as is indicated by the splitting pattern (Fig. 5c). The Q-band ENDOR spectra at the low-field position (Fig. 5d) show a well-resolved doublet centered at $A_z/2$ with a negligible nuclear quadrupole splitting. The hyperfine and nuclear quadrupole values obtained from simulations are given in Table 2.

To determine the magnetic parameters of the remote nitrogens of the macrocycle, HYSCORE spectra at X-band were recorded (not shown). All spectra show two diagonal peaks in the $(+,+)$ quadrant at low frequencies. The diagonal peak at (3.12,3.12) MHz is attributed to weakly coupled carbons in natural abundance, whereas the diagonal peak at (3.61,3.61) MHz does not fit any of the expected nuclear Zeeman frequencies. We assume that this peak stems from interactions with the remote nitrogens of the Pc ring, with hyperfine couplings close to zero. For weakly coupled nitrogens the strongest cross-peaks in a HYSCORE spectrum, correlate in general to the two double-quantum (DQ) frequencies,

$$\nu_{\alpha,\beta}^{DQ} = 2\sqrt{(a/2 \pm \nu_I)^2 + K^2(3+\eta)^2}, \qquad (3)$$

where a is the hyperfine coupling at the observer position, ν_I is the nuclear Zeeman frequency and K and η have been defined earlier. For a very small hyperfine interaction, $\nu_\alpha^{DQ} \approx \nu_\beta^{DQ}$, which leads to a value of $K(3 + \eta^2) = 2.5$ MHz for the remote nitrogens. With $0 < \eta < 1$, we find 3.65 MHz $> |e^2qQ/h| >$ 3.16 MHz, in good agreement with nuclear quadrupole resonance data of the bi-coordinated nitrogen in *l*-histidine ($|e^2qQ/h| = 3.267$ MHz, $\eta = 0.129$).[48] Fig. 6 shows the X-band proton-ENDOR spectra of CuPc and $CuPc^t$ in sulfuric acid and toluene and in the corresponding deuterated solvents

Table 1 The g and A^{Cu} principal values of CuPc and CuPc^t in various matrices in comparison with different Cu^{II} porphyrin and phthalocyanine complexes (hyperfine values (in MHz) given for the ^{63}Cu isotope)

	$g_\perp$	$g_\parallel$	$A_\perp^{Cu\ 45}$	$A_\parallel^{Cu\ 45}$	Ref.
CuPc^t–toluene	2.0405[a]	2.1625[a]	−86[b]	−643[b]	This work
CuPc^t–H_2SO_4	2.0525[a]	2.1994[a]	−54[b]	−608[b]	This work
CuPc–H_2SO_4	2.0520[a]	2.1990[a]	−52[b]	−616[b]	This work
CuPc–H_2Pc powder	2.0390[a]	2.1577[a]	−83[b]	−648[b]	This work
CuPc–H_2Pc powder	2.060	2.179	−80	−637	45
CuPc^t–toluene	2.048	2.163	−96	−636	12
CuPc^t–toluene	2.045	2.162	−90	−651	15
CuPc–H_2SO_4	—	2.168	—	−588	14
CuPc/H_2SO_4	2.045	2.175	−96	−606	17
CuPc–H_2SO_4	2.062	2.20	−54	−646.50	18
CuTPP single crystal	2.045	2.190	−102.7	−615	46
CuTPP–toluene-d_6	2.055	2.186	−98.6	−631	45

[a] Experimental error 0.0005. [b] Experimental error 3 MHz.

observed at the field position $\boldsymbol{B}_0 \parallel \boldsymbol{g}_\perp$. The Davies-ENDOR spectra are recorded using weak mw pulses to suppress the signal of the strongly coupled isoindole nitrogens. Upon deuteration of the solvent some of the proton signals disappear, indicating that these features represent hyperfine interactions with protons of the solvent. The remaining signals are due to the interactions with protons of the macrocycle. The broad shoulders in the proton-ENDOR spectra of CuPc and CuPc^t in sulfuric acid (Fig. 6d and e) arise from the hyperfine interaction of the protons attached to the bridging aza nitrogen nuclei. Upon dissolving the compounds in deuterated sulfuric acid these features disappear (Fig. 6a and b). As the protonation of the meso nitrogen nuclei is not expected in the case of CuPc and CuPc^t in toluene, the broad features in Fig. 6f have to be assigned to another interaction. A coordination of solvent molecules to the phthalocyanine complex, *e.g.* by π–π stacking, could account for this observation. This π-interaction between various aromatic groups and the porphyrins ring has been documented.[49] This hypothesis is supported by the shoulders which are lacking in the spectrum of CuPc^t in deuterated toluene (Fig. 6c). Furthermore, a peak at the proton Zeeman frequency ν_H is observed for CuPc (Fig. 6d) and CuPc^t in H_2SO_4 and toluene (Fig. 6e and f), which disappears upon deuteration of the solvents. This signal represents a large number of distant solvent protons. From the ENDOR spectra of CuPc in D_2SO_4 (Fig. 6a) the hyperfine interactions of the octa-peripheral and octa-nonperipheral protons can be determined (Table 3).

Experimental and simulated ENDOR spectra are shown in Fig. 7a and b. Furthermore, comparison of the ENDOR spectra of CuPc and CuPc^t in D_2SO_4 reveals a coupling of 0.4 MHz that can be attributed to the *tert*-butyl groups in agreement with the findings from DFT calculations. Finally, a comparison of the spectra in Fig. 6b and c shows that the hyperfine interaction with the protons of the phthalocyanine is only slightly dependent on the solvent. Fig. 7c shows the Mims-ENDOR spectrum of CuPc^F in D_2SO_4 taken at

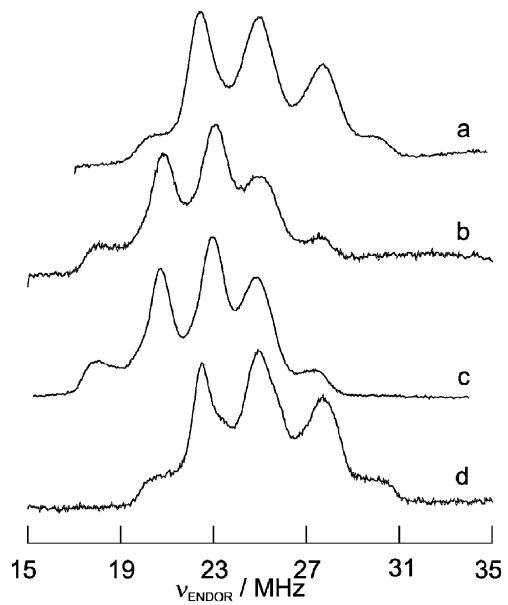

Fig. 4 Experimental X-band nitrogen Davies-ENDOR spectra, pulse lengths (52/26/52 ns), recorded at observer position $g_\perp$. (a) CuPc^t in toluene. (b) CuPc^t in H_2SO_4. (c) CuPc in H_2SO_4. (d) CuPc in H_2Pc.

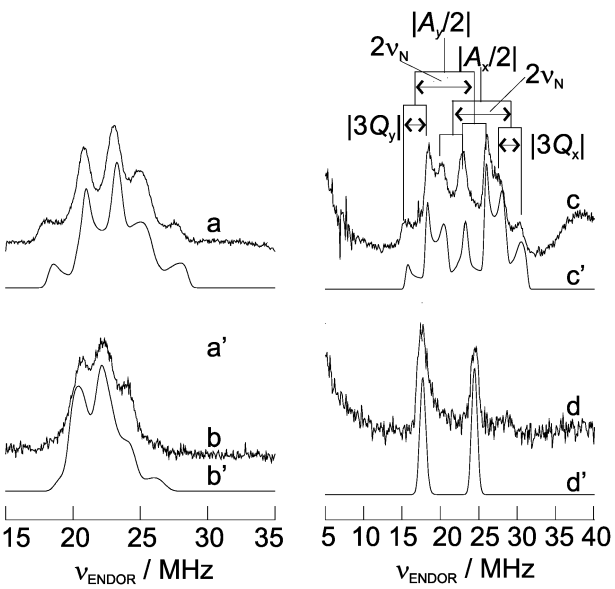

Fig. 5 Experimental and simulated X- and Q-band nitrogens Davies-ENDOR spectra pulse lengths (40/20/40 ns). (a) X-Band, observer position $g_\perp$. (b) X-Band, observer position at $g_\parallel$. (c) Q-Band, observer position $g_\perp$. (d) Q-Band, observer position $g_\parallel$. The simulated spectra are denoted by a′, b′, c′, and d′.

Table 2 ^{14}N hyperfine and nuclear quadrupole parameters of the isoindole nitrogens for different Cu^{II} phthalocyanine and Cu^{II} porphyrin systems used in the simulations of the X- and Q-band ENDOR spectra (in MHz)

	A_x	A_y	A_z	Q_x	Q_y	Q_z	Ref.
$CuPc^t$–toluene	56.4[a]	44.8[a]	45.7[a]	−0.790[b]	0.820[b]	−0.030[b]	This work
$CuPc^t$–H_2SO_4	52.4[a]	41.2[a]	41.8[a]	−0.882[b]	0.995[b]	−0.113[b]	This work
CuPc–H_2SO_4	51.4[a]	40.8[a]	41.0[a]	−0.878[b]	0.998[b]	−0.120[b]	This work
CuPc–H_2Pc powder	56.5[a]	44.7[a]	45.4[a]	−0.760[b]	0.765[b]	−0.005[b]	This work
CuTPP single crystal	54.2	42.8	44.06	−0.619	0.926	−0.307	46
CuTPP–toluene-d_6	54.2	42.6	42.6	−0.696	0.826	−0.130	45
CuPc–H_2Pc powder	57.2	42.0	42.08	−0.800	0.950	−0.150	45

[a] Experimental error 0.2 MHz. [b] Experimental error 0.005 MHz.

observer position $\boldsymbol{B}_0 \parallel \boldsymbol{g}_\perp$ together with the corresponding simulations.

The spectrum represents the hyperfine interactions of the ^{19}F nuclei, which allows for an assignment of the spin density at the octa-peripheral (p) and octa-nonperipheral (np) positions of the Pc^F ring. The peak marked by (*) in Fig. 7c corresponds to proton interactions. Since deuterated sulfuric acid (>99.6%) was used, these proton signals probably arise from proton impurities in the solvent. Note that the EPR spectrum of $CuPc^F$ in sulfuric acid showed the presence of a second unidentified Cu^{II} complex, which could not be removed by sublimation. This is in accordance with our earlier observations using UV/Vis spectroscopy. The ENDOR spectra shown here are taken at field positions where the second component did not contribute to the spectrum.

Assuming the spin-density distribution in the macrocycle remains unchanged when going from CuPc to $CuPc^F$, the ^{19}F hyperfine values can be estimated from the corresponding proton hyperfine values. The isotropic part of the hyperfine interaction scales as $a_{iso}^F = a_{iso}^H$ (49910/1420).[50] We would therefore expect large ^{19}F couplings ($a_{iso}(F(1)) \sim 16.5$ MHz, $a_{iso}(F(2)) \sim -1.68$ MHz). However, such couplings are not observed, indicating that the spin-density distributions in CuPc and $CuPc^F$ are different. Fig. 7c' shows a good fit of the spectrum using the parameters in Table 3.

Finally, it should be noted that CuPc could only be diluted in metal-free phthalocyanine using vacuum sublimation[11,26,27] (see Experimental). The cw-EPR spectrum of CuPc–H_2Pc obtained by a simple co-precipitation shows the same features as the spectrum of CuPc in sulfuric acid. Furthermore, the ENDOR analysis showed the presence of acidic protons in this sample. In view of this finding, one should be very cautious when interpreting data from the literature. Greiner *et al.*,[45] for instance, prepared a CuPc–H_2Pc sample without using the sublimation technique.

In order to elucidate some of the experimental observations, DFT computations of the magnetic parameters of CuPc, $CuPc^t$ and $CuPc^F$ have been carried out. We have to emphasize that the precision of DFT computations with the present functionals is not overwhelming and quantitative agreement with the experimental data cannot be expected. The DFT results will therefore only be used to check experimentally observed trends. Tables 4–6 show the computed copper, ^{14}N, ^1H and ^{19}F hyperfine data for the different complexes. The hyperfine tensors are visualized in Fig. 8.

The DFT results confirm that a change of the periphery of the phthalocyanine macrocycle has little influence on the copper and isoindole nitrogen hyperfine values as found experimentally (compare results in Table 4 and experimental data of CuPc and $CuPc^t$ in H_2SO_4). The experimental trends observed for the copper hyperfine values upon changing the polarity of the solvents could not be reproduced by the DFT

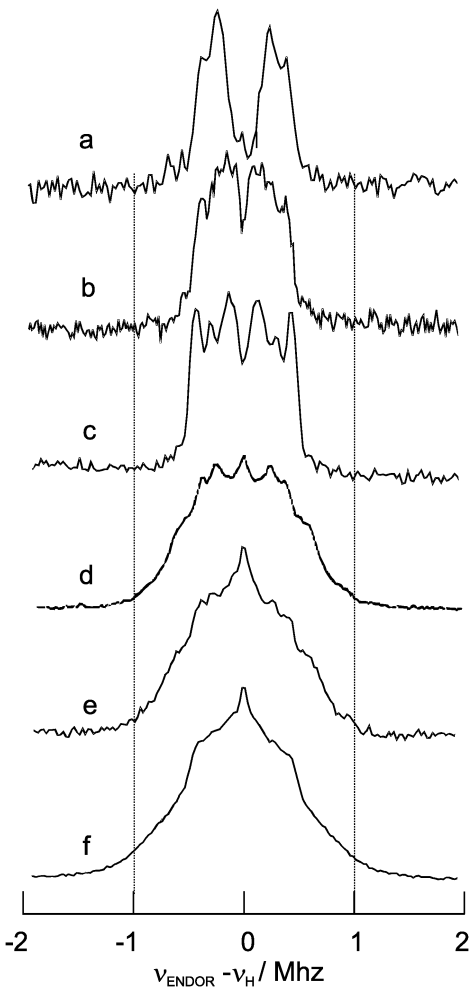

Fig. 6 X-Band proton Davies-ENDOR spectra, pulse lengths (400/200/400 ns), recorded at observer position $g_\perp$. (a) CuPc in D_2SO_4, (b) $CuPc^t$ in D_2SO_4, (c) $CuPc^t$ in d_8-toluene, (d) CuPc in H_2SO_4, (e) $CuPc^t$ in H_2SO_4 and (f) $CuPc^t$ in toluene.

Table 3 Principal values (in MHz) of the proton and fluorine hyperfine interactions of the p and np nuclei of CuPc and $CuPc^F$ in D_2SO_4 and Cu–H. Cu–F distances are given in Å, and x' and y' lie in the Pc plane, whereas z' points along the normal of the plane. It is assumed that x' lies along the Cu–H (Cu–F) direction

Nucleus	A_x	A_y	A_z	a_{iso}	r	r (X-ray)[46]
H(p)[a]	0.85	0.37	0.25	0.49	7.9	8
H(np)[a]	0.85	−0.5	−0.5	−0.05	5.7	5.6
F(p)[b]	1.1	0.7	0.4	0.7	8.3	—
F(np)[b]	1.3	0.3	0.3	0.6	6.1	—

[a] Experimental error 0.08 MHz. [b] Experimental error 0.1 MHz.

results. Nevertheless, toluene modelling correctly leads to a lower value of $|e^2qQ/h|$ of the isoindole nitrogen than sulfuric acid modelling and the trend for η is in agreement with the one observed experimentally (compare Table 4 and Table 5). Comparison of Tables 3 and 6 gives confidence in the assignment of the n and np proton hyperfine interactions of CuPc in D_2SO_4. Furthermore, the ^{19}F hyperfine values computed for $CuPc^F$ are clearly smaller than those expected from a simple extrapolation of the proton data of CuPc. This corroborates the experimental observations and confirms that no fluorine signals were missed in the ENDOR spectra.

Discussion

Motional behaviour of the CuPc complexes in solution

The X-band solution EPR spectrum of $CuPc^t$ in toluene recorded at room temperature (Fig. 3a) shows the four-line pattern expected for a coupling of an electron spin with a nucleus with spin $I = 3/2$ (Cu) with well-resolved lines for $m_I = +3/2$ and $+1/2$. The linewidth becomes larger at lower m_I values (m_I dependence of the linewidth, $\Gamma = A + Bm_I + Cm_I^2$).[51] At room temperature, the molecular motion of $CuPc^t$ and CuPc in sulfuric acid in a flat cell and in a capillary (Fig. 3b and c) is about three orders of magnitude slower than that of $CuPc^t$ in toluene. The cooling experiment (Fig. 3d–f) revealed that at room temperature, the rotation around the in-plane axes is slow, whereas rotation around the z-axis is still possible. This rotation is stopped upon freezing, resulting in the usual powder spectrum for $T < 235$ K (Fig. 3f). This motional behaviour, which is only observed in sulfuric acid and could be well simulated in the slow motion regime, can be mainly ascribed to the large viscosity of this solvent.

Interpretation of the EPR parameters

The delocalization of the unpaired electron spin over the complex can be studied in order to probe the energetic state of a molecule, as a change in the spin density distribution is the direct consequence of a change in the energy levels. Thus, a careful analysis of the experimental EPR data provides deeper insight into the chemical behaviour of the investigated compound. These data are important in order to understand how peripheric ring substitutions and solvent effects can modulate the catalytic properties of the phthalocyanine complexes, *e.g.* by changing the characteristics for axial ligation.

The $\boldsymbol{g}$ and $\boldsymbol{A}^{Cu}$ matrices of CuPc and $CuPc^t$ are axially symmetric, reflecting the D_{4h} core symmetry in the molecules. The four isoindole nitrogens are equivalent within the experimental error of the ENDOR experiments. The principal values of the matrices $\boldsymbol{g}$ and $\boldsymbol{A}^{Cu}$ are given in Table 1. The observation that $g_\parallel > g_\perp$ and $|A_\parallel| > |A_\perp|$ implies a B_{1g} ground state. The ground state as well as the symmetry correspond to the DFT results. Using the definition of the x and y axes given in

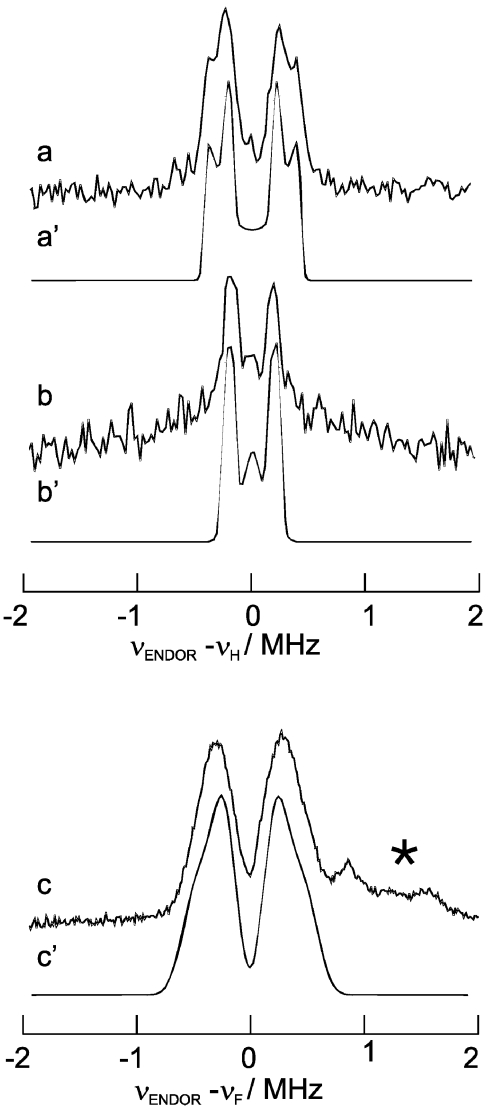

Fig. 7 Experimental and simulated X-band proton Davies-ENDOR spectra, pulse lengths (400/200/400 ns). (a) and (b) CuPc in D_2SO_4. (a,a′) Observer position $g_\perp$. (b,b′) Observer position $g_\parallel$. (c) Experimental X-band fluorine Mims-ENDOR spectrum of $CuPc^F$ in D_2SO_4, observer position $g_\perp$. (c′) Simulation of (c).

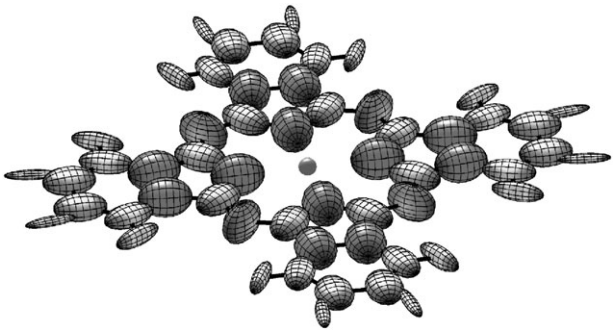

Fig. 8 Visualization of the hyperfine tensors of the CuPc complex. Both the form of the ellipsoids and the mapping represent the full tensor. The sizes of the tensors have been normalized.

Fig. 1, the relevant molecular orbitals with D_{4h} symmetry are[16–17,47,52]

$$b_{1g} = \alpha d_{x^2-y^2} - \frac{\alpha'}{2}(-\sigma_1^x + \sigma_2^y + \sigma_3^x - \sigma_4^y), \quad (4)$$

$$b_{2g} = \beta d_{xy} - \frac{\beta'}{2}(\pi_1^y + \pi_2^x - \pi_3^y - \pi_4^x), \quad (5)$$

$$a_{1g} = \varepsilon d_{z^2} - \frac{\varepsilon'}{2}(\sigma_1^x + \sigma_2^y - \sigma_3^x - \sigma_4^y), \quad (6)$$

$$e_g = \begin{bmatrix} \delta d_{xz} - \frac{\delta'}{\sqrt{2}}(\pi_1^z - \pi_3^z) \\ \delta d_{yz} - \frac{\delta'}{\sqrt{2}}(\pi_2^z - \pi_4^z) \end{bmatrix}. \quad (7)$$

The b_{1g} and a_{1g} orbitals account for the σ bonding to the metal, and b_{2g} represents the in-plane and e_g the out-of-plane π bonding. Subscripts 1 and 3 (2 and 4) denote the nitrogens on the *xy* axis. The *g* and copper hyperfine values can then be expressed as

$$g_\parallel = 2.0023 - \frac{8\lambda\alpha^2\beta^2}{\Delta(b_{2g} - b_{1g})} \quad (8)$$

$$g_\perp = 2.0023 - \frac{2\lambda\alpha^2\delta^2}{\Delta(e_g - b_{1g})} \quad (9)$$

$$A_\parallel = P\left(-\kappa - \frac{4}{7}\alpha^2 + \Delta g_\parallel + \frac{3}{7}\Delta g_\perp\right), \quad (10)$$

$$A_\perp = P\left(-\kappa + \frac{2}{7}\alpha^2 + \frac{11}{14}\Delta g_\perp\right) \quad (11),$$

where $\lambda = -830$ cm^{-1} is the spin–orbit coupling constant of the free copper(II) ion,[53] $-P\kappa$ is the Fermi contact term, $P = \beta_e\beta_n g_e g_n \langle r^{-3}\rangle = 1164$ MHz ($^{63}Cu^{II}$)[53] is the dipolar hyperfine coupling parameter of the unpaired electron and $\Delta g_{\parallel,\perp} = g_{\parallel,\perp} - 2.0023$.

From eqn (10) and (11) and the experimental copper hyperfine couplings, the values for κ and α^2 can be determined (Table 6). The parameter α^2 is a covalency parameter, which describes the in-plane metal–ligand σ bonding. For pure ionic bonding, $\alpha^2 = 1$, for covalent bonding $\alpha^2 < 1$. For the Cu^{II} complexes under study, α^2 is found to vary between 0.72 and 0.77 and κ is in the range 0.28–0.31. This agrees with values

Table 4 Computed copper hyperfine values (in MHz) for the different Cu^{II} phthalocyanine complexes and spin population of copper. The data should be compared with Table 1. For the visualization of the hyperfine tensors, see Fig. 8

	A_x /MHz	A_y /MHz	A_z /MHz	ρ^{Cu}
CuPc/vacuo	−20	−20	−612	0.54
CuPc–H_2SO_4	9.3	9.7	−630	0.61
$CuPc^F$/vacuo	−18	−19	−613	0.54
$CuPc^F$–H_2SO_4	13.3	14.7	−632	0.62
$CuPc^t$–toluene	−15	−15	−615	0.55
$CuPc^t$–H_2SO_4	8.9	9.4	−630	0.61

reported earlier for other copper complexes.[47] The values of α^2 indicate that approximately 74% of the spin population is in the copper $d_{x^2-y^2}$ orbital. The b_{1g} orbital is quite covalent in nature. This result contradicts earlier DFT computations on CuPc systems where α^2 was predicted to be only 44%.[54] These values are also lower than those found in our present DFT analysis (54–62%, Table 4).

When comparing the values of α^2 for $CuPc^t$ in sulfuric acid and toluene, it becomes clear that the metal–nitrogen bond is less covalent in the case of sulfuric acid. This may be caused by the protonation of the meso nitrogens,[37–40] which increases the ionicity in the metal–nitrogen bond. Normalization of the b_{1g} orbital yields

$$\alpha^2 + \alpha'^2 - 2\alpha\alpha' S = 1, \quad (12)$$

with the overlap integral

$$S = \langle d_{x^2-y^2}(-\sigma_1^x + \sigma_2^y + \sigma_3^x - \sigma_4^y)\rangle/2 = 2\langle d_{x^2-y^2}|(-\sigma_1^x)\rangle. \quad (13)$$

The overlap integral was earlier determined to be $S = 0.093$.[17] Eqn (12) allows for the determination of the $(\alpha'/2)^2$ values from the α^2 values. They are also given in Table 6. To determine the energy splittings $\Delta(b_{2g}–b_{1g})$ and $\Delta(e_g–b_{1g})$ from the experimental *g* values using eqn (8) and (9), the covalency parameters of the in-plane π bonding (β^2) and the out-of-plane π bonding (δ^2) have to be known. A first guess of these parameters can be obtained indirectly from the analysis of the hyperfine values of the isoindole nitrogens.

From X-ray studies on β-polymorphous CuPc a Cu–N distance of $r = 1.934$ Å has been found.[55] Using this distance, the point-dipole part of the nitrogen hyperfine matrix can be calculated using eqn (2) with $\phi = 90°$. As the Cu–N bonds are along $g_\perp$, the principal axes frame of the point-dipole contribution and the ***g*** principal axis frame are not tilted. The hyperfine matrix of the isoindole nitrogens can then be split into an isotropic part a_{iso} and three anisotropic contributions. In the following partitioning of the hyperfine principal values, the first term describes the isotropic hyperfine interaction, and the second one the aforementioned point-dipole contribution. The latter is orthorhombic and not traceless because of the ***g*** anisotropy.[19] This term therefore has to be deduced first from the full hyperfine matrix, after which the isotropic part can be calculated as one third of the trace of the remaining part. After subtraction of the isotropic part the remainder is separated into the second and third anisotropic terms arising from the metal–ligand σ bonding (in the plane with the largest value along the Cu–N bond) and from the out-of-plane π bonding

Table 5 Computed hyperfine and nuclear quadrupole parameters (in MHz) of the isoindole nitrogens of different Cu^{II} phthalocyanine complexes. The value ρ_N is the s-orbital spin population on each of the isoindole nitrogens. This table should be compared with Table 2. For the visualization of the hyperfine tensors, see Fig. 8

	A_x	A_y	A_z	Q_x	Q_y	Q_z	η	ρ^N
CuPc/vacuo	63	50	48	−0.74	0.90	−0.16	0.64	0.023
CuPc–H_2SO_4	60	48	47	−0.80	1.09	−0.29	0.47	0.022
$CuPc^F$/vacuo	62	49	48	−0.71	0.91	−0.20	0.55	0.022
$CuPc^F$–H_2SO_4	58	47	46	−0.82	1.12	−0.29	0.47	0.021
$CuPc^t$–toluene	62	49	48	−0.76	0.92	−0.16	0.65	0.022
$CuPc^t$–H_2SO_4	59	48	47	−0.80	1.10	−0.31	0.44	0.022

(perpendicular to the complex plane). A fourth anisotropic term describing the in-plane π bonding cannot be derived from solving the underlying linear equations.

We find for $CuPc^t$ in toluene

$$\begin{bmatrix}56.4\text{ MHz}\\44.8\text{ MHz}\\45.7\text{ MHz}\end{bmatrix} = 48.98\text{ MHz} + \begin{bmatrix}1.62\text{ MHz}\\-0.81\text{ MHz}\\-0.85\text{ MHz}\end{bmatrix} + \begin{bmatrix}6.10\text{ MHz}\\-3.05\text{ MHz}\\-3.05\text{ MHz}\end{bmatrix} + \begin{bmatrix}-0.32\text{ MHz}\\-0.32\text{ MHz}\\0.64\text{ MHz}\end{bmatrix}, \quad (14)$$

for $CuPc^t$ in sulfuric acid

$$\begin{bmatrix}52.4\text{ MHz}\\41.2\text{ MHz}\\41.8\text{ MHz}\end{bmatrix} = 45.35\text{ MHz} + \begin{bmatrix}1.63\text{ MHz}\\-0.80\text{ MHz}\\-0.87\text{ MHz}\end{bmatrix} + \begin{bmatrix}5.44\text{ MHz}\\-2.72\text{ MHz}\\-2.72\text{ MHz}\end{bmatrix} + \begin{bmatrix}-0.20\text{ MHz}\\-0.20\text{ MHz}\\0.40\text{ MHz}\end{bmatrix}, \quad (15)$$

for CuPc in sulfuric acid

$$\begin{bmatrix}51.4\text{ MHz}\\40.8\text{ MHz}\\41.0\text{ MHz}\end{bmatrix} = 44.42\text{ MHz} + \begin{bmatrix}1.63\text{ MHz}\\-0.82\text{ MHz}\\-0.87\text{ MHz}\end{bmatrix} + \begin{bmatrix}5.48\text{ MHz}\\-2.74\text{ MHz}\\-2.74\text{ MHz}\end{bmatrix} + \begin{bmatrix}-0.09\text{ MHz}\\-0.09\text{ MHz}\\0.18\text{ MHz}\end{bmatrix} \quad (16),$$

and for CuPc in H_2Pc

$$\begin{bmatrix}56.5\text{ MHz}\\44.7\text{ MHz}\\45.4\text{ MHz}\end{bmatrix} = 48.90\text{ MHz} + \begin{bmatrix}1.62\text{ MHz}\\-0.81\text{ MHz}\\-0.86\text{ MHz}\end{bmatrix} + \begin{bmatrix}6.22\text{ MHz}\\-3.11\text{ MHz}\\-3.11\text{ MHz}\end{bmatrix} + \begin{bmatrix}-0.23\text{ MHz}\\-0.23\text{ MHz}\\0.46\text{ MHz}\end{bmatrix}. \quad (17)$$

From the Fermi contact term, the spin density ($\rho^N = a_{iso}/a_0$ with $a_0 = 1538.22$ MHz[56]) on each of the isoindole nitrogen nuclei is calculated. The ρ^N values (Table 6) correlate nicely with the values of $(\alpha'/2)^2$ ($\rho^N \approx 1/3(\alpha'/2)^2$) and the s-orbital spin densities on the nitrogen nuclei obtained by DFT calculations (Table 5, Fig. S4 and ESI†). Since the atomic σ orbitals in eqn (13) are sp^2 hybrids, the theory given above is confirmed. No contribution from in-plane π bonding is found ($\beta' \approx 0$), suggesting a true sp^2 hybridization. This confirms earlier results[10,16] but contradicts the work of Kivelson and Neiman, who derived from their EPR data a marked covalency of the in-plane π bonding and postulated this bonding to be the origin for the large stability of the metal phthalocyanines.[17] Our DFT computations show that there is some in-plane π bonding, but that it does not contribute to the SOMO and is thus not reflected in the EPR parameters. Substitution of $\beta^2 \approx 1$ in eqn (8) allows one to estimate the $\Delta(b_{2g}–b_{1g})$ transition energy (Table 6). The calculated values agree with the absorption band observed at 33 300 cm^{-1} in CuPc.[57] This absorption band was earlier also assigned to the $\Delta(b_{2g}–b_{1g})$ transition.[10] Furthermore, the calculated values agree with those derived for other Cu^{II} complexes.[47] The addition of sulfuric acid reduces $\Delta(b_{2g}–b_{1g})$, which is in good agreement with the result obtained by comparing the DFT data of the complexes protonated at the meso positions with the non-protonated ones.

Eqn (14)–(17) indicate that a significant out-of-plane π bonding takes place ($\delta'^2 > 0$, $\delta^2 < 1$). The covalency of this bonding increases upon addition of *tert*-butyl substituents. Furthermore, the polar sulfuric acid environment reduces the covalency in comparison to the nonpolar toluene or to the H_2Pc environment. The data can further be analyzed by calculating the out-of-plane π-bonding parameter δ^2 by inserting in eqn (9) the two possible values for the energy of the $\Delta(e_g–b_{1g})$ absorption band taken from the experimental UV/Vis spectrum of CuPc in sulfuric acid (14 970 and 15 723 cm^{-1}). This yields $\delta^2 = 0.58$ and 0.61, respectively.

Table 2 shows that the nitrogen nuclear quadrupole interaction is also very sensitive to the environment of CuPc. Since the electric field gradient depends on the total electron density, it is not surprising that the change from a nonpolar surrounding (toluene, H_2Pc) to sulfuric acid induces a change of the asymmetry parameter and an increase of $|e^2qQ/h|$. Both effects are nicely reproduced by our DFT computations using solvent modelling and including the protonation of the meso nitrogen nuclei. Furthermore, the nuclear quadrupole interaction of the isoindole nitrogens in CuPc is more asymmetric than that of the pyrrole nitrogens in copper(II) tetraphenylporphyrin

Table 6 Parameters derived from the EPR data of the different CuPc complexes. $P\kappa$ = Fermi contact term, α^2 = covalency parameter, ρ^N = spin population on each of the isoindole nitrogens, $\Delta(b_{2g}–b_{1g})$ = energy splitting

	κ	α^2	$(\alpha'/2)^2$	ρ^N	$\Delta(b_{2g}–b_{1g})$ /cm^{-1} [a]
$CuPc^t$–toluene	0.310	0.729	0.0919	0.0318	30 374
$CuPc^t$–H_2SO_4	0.304	0.763	0.0825	0.0293	25 831
CuPc–H_2SO_4	0.305	0.773	0.0799	0.0289	26 215
CuPc–H_2Pc powder	0.309	0.731	0.0913	0.0318	31 414

[a] Derived from eqn (8) and $\beta^2 = 1$.

Table 7 Computed principal values of the proton and fluorine hyperfine interactions (in MHz) of the p and np nuclei of CuPc and $CuPc^F$ *in vacuo* and sulfuric acid, Cu–H, Cu–F distances (in Å) and spin population on proton or fluorine

Nucleus	A_x	A_y	A_z	a_{iso}	r^{50}	$\rho^{H/F}$
Vacuo: H(p)	0.72	0.19	0.12	0.34	7.65	0.0003
Vacuo: H(np)	1.00	−0.29	−0.38	0.10	5.95	0.0000
H_2SO_4: H(p)	0.71	0.20	0.13	0.34	7.60	0.0002
H_2SO_4: H(np)	0.87	−0.37	−0.44	0.02	5.99	0.0000
H_2SO_4: H(NH)	−1.78	−1.41	1.40	−0.60	4.36	−0.0003
Vacuo: F(p)	2.70	0.71	−0.18	1.06	7.92	0.0001
Vacuo: F(np)	1.25	0.97	−0.46	0.59	6.12	0.0001
H_2SO_4: F(p)	1.95	0.41	−0.64	0.57	7.94	0.0001
H_2SO_4: F(np)	1.16	0.55	−0.69	0.34	6.16	0.0000
H_2SO_4: F(NH)	−1.71	−1.36	1.42	−0.55	4.37	−0.0002

(CuTPP).[46] This may be because CuPc is a more rigid molecule, while the macrocycle in CuTPP could be more flexible. The absolute signs of the nuclear quadrupole couplings cannot be determined from the experiment. Brown and Hoffman[46] showed that for CuTPP the largest nuclear quadrupole coupling is negative and oriented along the metal–N bond, whereas its value is positive when it is perpendicular to this bond but parallel to the heterocycle plane. Together with our DFT data, this justifies the choice of the signs of the $\boldsymbol{Q}$ principal values.

The hyperfine interactions with the p and np protons (Table 3) are obtained from the ENDOR spectra of CuPc in deuterated sulfuric acid. The distances determined from the point-dipole part of the hyperfine matrix are in agreement with the X-ray data (p protons: 7.9 Å, np protons: 5.7 Å).[55] The spin population on the Pc protons is caused by the conjugation of the ring π system and agrees with a single crystal ENDOR study of CuTPP, which revealed a hyperfine interaction of about (2.5, 0.7, 0.8) MHz of the β-protons of the porphyrin ring.[46] Since in CuTPP the β-protons are closer to the Cu^{II} ion, the a_{iso} values and point-dipole interactions are larger for the protons in CuPc. Furthermore, DFT computations (Table 7) corroborate the experimental assignment. The isotropic hyperfine couplings for the fluorine nuclei of $CuPc^F$ deviate strongly from those predicted based on the proton hyperfine values in CuPc. This might be due to a compensation of the direct s-spin density by spin-polarization effects. Spin polarization is not uncommon when π bonding is involved and the p-orbitals of the fluorine atoms may take part in the π-bonding system of the macrocycle, which is confirmed by the results of our DFT calculations (Table 7). The s-orbital spin population of the p protons in CuPc is around 0.0002 and it is below the detection limit for the np protons. In the case of $CuPc^F$ the situation is slightly different: the main contribution to the spin population of the p-fluorine nuclei arises from the p-orbitals, whereas it is a combination of s- and p-contribution for the np nuclei.

Analysis of the proton-ENDOR spectra of $CuPc^t$ in protonating and deuterating solvents indicates that in sulfuric acid the largest observed proton hyperfine interactions stem from the protons attached to the meso nitrogens whereas in toluene this interaction could be assigned to solvent protons. This again shows that the copper(II) ion senses the matrix environment. Finally, the difference in the proton-ENDOR spectra of $CuPc^t$ and CuPc in sulfuric acid illustrates the power of ENDOR in detecting small influences of substituents.

Conclusions

Our study shows that the environment and the ring substituents have a remarkable effect on the spin density distribution in CuPc and thus influence the catalytic activity as well as the color of the complex. Both features are important for industrial applications of the Pc complexes. Furthermore, our analysis shows that advanced EPR and ENDOR methods are excellent tools for monitoring these effects and that the spectral interpretation can be facilitated using DFT computations. The results should act as a stimulus for a more regular use of these methods in the characterization of newly-synthesized paramagnetic metal complexes. Moreover, the detection of sulfuric acid in CuPc diluted in H_2Pc indicates that the methods can also be successfully used in optimizing purification processes.

Acknowledgements

We gratefully acknowledge the financial support of the Swiss National Science Foundation. We are also grateful to Dr Igor Gromov for his assistance during the Q-band ENDOR measurements and to Walter Lämmler who purified the CuPc samples.

References

1 P. Kivits, R. Debont and J. Vanderveen, *Appl. Phys. A: Mater. Sci. Process.*, 1981, **26**, 101–105.
2 K. Kasuga, M. Terauchi, M. Hara, K. Nishie, T. Sugimori and M. Handa, *Bull. Chem. Soc. Jpn.*, 1997, **70**, 2107–2110.
3 J. A. Thompson, K. Murata, D. C. Miller, J. L. Stanton, W. E. Broderick, B. M. Hoffman and J. A. Ibers, *Inorg. Chem.*, 1993, **32**, 3546–3553.
4 F. H. Moser and A. L. Thomas, *Phthalocyanine Compounds (ACS Monograph 157)*, Oxford University Press, New York, 1963.
5 F. Baumann, B. Bienert, G. Rosch, H. Vollmann and W. Wolf, *Angew. Chem., Int. Ed. Engl.*, 1956, **68**, 133–150.
6 N. B. McKeown, *Phthalocyanine Materials: Structure, Synthesis, and Function*, Cambridge University Press, Cambridge, 1998.
7 J. R. Darwent, P. Douglas, A. Harriman, G. Porter and M. C. Richoux, *Coord. Chem. Rev.*, 1982, **44**, 83–126.
8 J. R. Darwent, *J. Chem. Soc., Faraday Trans. 2*, 1981, **77**, 1703–1709.
9 P. C. Rieke and N. R. Armstrong, *J. Am. Chem. Soc.*, 1984, **106**, 47–50.
10 C. M. Guzy, J. B. Raynor and M. C. R. Symons, *J. Chem. Soc. A*, 1969, 2299.
11 M. Abkowitz, I. Chen and J. H. Sharp, *J. Chem. Phys.*, 1968, **48**, 4561.
12 R. Heucher, G. V. R. Chandramouli and P. T. Manoharan, *J. Porphyrins Phthalocyanines*, 1998, **2**, 423–427.

13 F. Koksal, F. Ucun, E. Agar and I. Kartal, *J. Chem. Res. (S)*, 1998, 96–97.
14 A. Graczyk and J. Dobkowski, *J. Magn. Reson.*, 1979, **34**, 467–474.
15 R. Rousseau, A. Ozarowski, R. Aroca, L. D. Soares and M. Trsic, *J. Mol. Struct.*, 1994, **317**, 287–297.
16 S. E. Harrison and J. M. Assour, *J. Chem. Phys.*, 1964, **40**, 365.
17 D. Kivelson and R. Neiman, *J. Chem. Phys.*, 1961, **35**, 149.
18 S. Seelan, M. S. Agashe, D. Srinivas and S. Sivasanker, *J. Mol. Catal. A: Chem.*, 2001, **168**, 61–68.
19 A. Schweiger and G. Jeschke, *Principles of pulse electron paramagnetic resonance*, Oxford University Press, New York, 1st edn, 2001.
20 A. Schweiger, *Angew. Chem., Int. Ed. Engl.*, 1991, **30**, 265–292.
21 C. Gemperle and A. Schweiger, *Chem. Rev.*, 1991, **91**, 1481–1505.
22 P. Höfer, A. Grupp, H. Nebenführ and M. Mehring, *Chem. Phys. Lett.*, 1986, **132**, 279–282.
23 E. R. Davies, *Phys. Lett. A*, 1974, **47**, 1–2.
24 W. B. Mims, *Proc. R. Soc. London, Ser. A*, 1965, **283**, 452.
25 I. Gromov, J. Shane, J. Forrer, R. Rakhmatoullin, Y. Rozentzwaig and A. Schweiger, *J. Magn. Reson.*, 2001, **149**, 196–203.
26 J. M. Assour and W. K. Kahn, *J. Am. Chem. Soc.*, 1965, **87**, 207.
27 D. N. Kendall, *Anal. Chem.*, 1953, **25**, 382–389.
28 G. H. Rist and J. S. Hyde, *J. Chem. Phys.*, 1970, **52**, 4633.
29 C. Gemperle, G. Aebli, A. Schweiger and R. R. Ernst, *J. Magn. Reson.*, 1990, **88**, 241–256.
30 S. Stoll and A. Schweiger, *J. Magn. Reson.*, 2006, **178**, 42–55.
31 E. J. Baerends, D. E. Ellis and P. Ros, *Chem. Phys.*, 1973, **2**, 41–51.
32 L. Versluis and T. Ziegler, *J. Chem. Phys.*, 1988, **88**, 322–328.
33 G. T. Velde and E. J. Baerends, *J. Comput. Phys.*, 1992, **99**, 84–98.
34 C. F. Guerra, J. G. Snijders, G. te Velde and E. J. Baerends, *Theor. Chem. Acc.*, 1998, **99**, 391–403.
35 E. vanLenthe, J. G. Snijders and E. J. Baerends, *J. Chem. Phys.*, 1996, **105**, 6505–6516.
36 A. Klamt and G. Schuurmann, *J. Chem. Soc., Perkin Trans. 2*, 1993, 799–805.
37 B. D. Berezin, *Zh. Fiz. Khim.*, 1961, **35**, 2494–2500.
38 W. Gunsser, R. Priess and B. Doscher, *Inorg. Chim. Acta*, 1980, **40**, X103–X103.
39 D. R. Stojakovic and N. Z. Rajic, *Inorg. Chim. Acta*, 1990, **171**, 17–20.
40 S. Gaspard, M. Verdaguer and R. Viovy, *J. Chem. Res. (S)*, 1979, 3072–3096.
41 *Knovel Critical Tables*, Knovel, 2003, http://www.knovel.com/knovel2/Toc.jsp?BookID = 761&VerticalID = 0.
42 S. Portmann and H. P. Lüthi, *Chimia*, 2000, **54**, 766–770.
43 G. C. Hurst, T. A. Henderson and R. W. Kreilick, *J. Am. Chem. Soc.*, 1985, **107**, 7294–7299.
44 M. Gouterman, in *The Porphyrins*, ed. D. Dophin, Academic Press, New York, 1977, vol. 3, pp. 1–157.
45 S. P. Greiner, D. L. Rowlands and R. W. Kreilick, *J. Phys. Chem.*, 1992, **96**, 9132–9139.
46 T. G. Brown and B. M. Hoffman, *Mol. Phys.*, 1980, **39**, 1073–1109.
47 M. Valente, C. Freire and B. de Castro, *J. Chem. Soc., Dalton Trans.*, 1998, 1557–1562.
48 M. J. Hunt, A. L. MacKay and D. T. Edmonds, *Chem. Phys. Lett.*, 1975, **34**, 473–475.
49 M. N. H. Williamson and C. L. Hill, *Inorg. Chem.*, 1987, **26**, 4155–4160.
50 *CRC Practical Handbook of Spectroscopy*, ed. J. W. Robinson, CRC Press, Boston, MA, 1991, p. 651.
51 A. Hudson and G. Luckhurst, *Chem. Rev.*, 1969, **69**, 191.
52 A. H. Maki and B. R. McGarvey, *J. Chem. Phys.*, 1958, **29**, 31–34.
53 M. J. Maroney, J. G. Norman and J. H. Osborne, *Inorg. Chem.*, 1984, **23**, 2261–2270.
54 M. S. Liao and S. Scheiner, *J. Chem. Phys.*, 2001, **114**, 9780–9791.
55 C. J. Brown, *J. Chem. Soc. A*, 1968, 2488–2493.
56 A. K. Koh and D. J. Miller, *At. Data Nucl. Data Tables*, 1985, **33**, 235–253.
57 P. E. Fielding and F. Gutman, *J. Chem. Phys.*, 1957, **26**, 411–419.